Fast preparation of *W* states with superconducting quantum interference devices by using dressed states

Yi-Hao Kang,[1] Ye-Hong Chen,[1] Zhi-Cheng Shi,[1] Jie Song,[2] and Yan Xia[1,*]

[1]*Department of Physics, Fuzhou University, Fuzhou 350002, China*
[2]*Department of Physics, Harbin Institute of Technology, Harbin 150001, China*

In this paper, we propose a protocol to prepare *W* states with superconducting quantum interference devices by using dressed states. Through choosing a set of dressed states suitably, the protocol can be used to accelerate the adiabatic passages while additional couplings are unnecessary. Moreover, we can optimize the evolution of the system with the restraint to the populations of the intermediate states by choosing suitable control parameters. Numerical simulations show that the protocol is robust against the parameter variations and decoherence mechanisms. Furthermore, the protocol is faster and more robust against the dephasing compared with that by the adiabatic passages. As for the Rabi frequencies of pulses designed by the method, they can be expressed by the linear superpositions of Gaussian functions, which does not increase difficulty in the experiments. In addition, the protocol could be controlled and manipulated easily in experiments with a circuit quantum electrodynamics system.

I. INTRODUCTION

Executing computation and communication tasks [1–4] in quantum-information processing (QIP) has become very attractive in recent years, since these tasks can be accurately completed with a suitable boundary condition of time-dependent interactions. For example, based on the idea of guiding the evolution of the system "riding" the adiabatic eigenstates from its initial state to the target state, adiabatic methods have been proposed and widely used successfully in many research fields, such as laser cooling and atom optics [5], metrology [6], interferometry [7], chemical reaction dynamics [8], and cavity quantum electrodynamics [9]. The most famous examples of adiabatic methods are the stimulated Raman adiabatic passages (STIRAP) method and its variants [8–11], which have shown many advantages. For instance, the protocols with the STIRAP method have great robustness against pulse area and timing errors. Moreover, when the system stays in the instantaneous ground state of its time-dependent Hamiltonian during the whole evolution process under an adiabatic control, the populations of the lossy intermediate states can be restrained so that the dissipation caused by decoherence, noise, and losses can be repressed. Although the adiabatic passages hold several advantages, the STIRAP methods require the system to be restricted by the adiabatic condition, which may greatly reduce the evolution speed of the system and make the system suffer more from the dissipation of its initial state and target state. For example, as shown in Refs. [12,13], by using STIRAP to create entanglement, the fidelities of obtaining the target states are very sensitive to the dephasing due to a long time evolution. It is generally known that, in the field of quantum computing and quantum-information processing, speed and precision are two primary factors. Therefore, in order to drive a system from a given initial state to a prescribed final state in a shorter time without losing the robustness property, a new sort of technique

called "shortcuts to adiabatic passages" (STAP) [14–23] has been put forward.

STAP aims at leading an adiabaticlike way between the system's initial state and the target state while the adiabatic condition is completely broken so that the evolution of the system can be accelerated a lot. Moreover, when a suitable boundary condition of time-dependent interactions is set, the robustness of STAP against parameter variations and decoherence mechanisms is also quite nice. Because of the attractive advantages, STAP has been applied in many kinds of research fields, e.g., fast cold atom, fast ion transport, fast quantum-information processing, fast wave-packet splitting, fast expansion, and so on [24–58]. Among these works [14–58], shortcut protocols [20–29] with the method transitionless quantum driving (TQD) are interesting. In these protocols [20–29], modifications of original Hamiltonians could be constructed to compensate for nonadiabatic errors by adding counterdiabatic driving (CDD) terms with TQD. However, as indicated in Ref. [59], the CDD terms sometimes play roles as either direct couplings between the initial state and the target state [20,60,61] or couplings not available in the original Hamiltonian [62]. It was shown in some previous protocols [25–29] that a direct coupling between the initial state and the target state may be hard to be realized in several cases, such as the special one-photon 1-3 pulse (the microwave field) for an atom transition. Therefore, many other interesting approaches [59,63–73] have been presented to construct STAP and avoid the issues caused by TQD. For example, Torrontegui *et al.* [66] used the dynamical symmetry of the Hamiltonian to find alternative Hamiltonians that achieved the same goals as speedup protocols via Lie transforms without directly using the counterdiabatic Hamiltonian. Ibáñez *et al.* [71] suggested to use iterative interaction pictures (also called multiple Schrödinger pictures) to obtain Hamiltonians with physically feasible structure for quantum systems. They also studied the capabilities and limitations of superadiabatic iterations to construct a sequence of shortcuts to adiabaticity by iterative interaction pictures [72]. Subsequently, the method with multiple Schrödinger pictures was expanded by

---

Song *et al.* [73] to a three-level system. They showed an interesting result in that the Hamiltonian in the second iteration of the interaction pictures has the same form as the Hamiltonian in the original Schrödinger picture [73]. Recently, Baksic *et al.* [59] proposed an interesting protocol about significantly speeding up adiabatic state transfers by using dressed states. Moreover, they have indicated in their article [59] that the populations of the intermediate states can be controlled by choosing one of the control parameters and such control is unavailable in the protocols with superadiabatic iterations. This result is quite attractive, since one can decrease the populations of the intermediate states by adjusting the corresponding parameters in order to reduce the dissipation of the intermediate states and improve the fidelity of obtaining the target state. Considering the advantages of the method by using dressed states, it is worthwhile to dig out the applications of this method for QIP in various physics systems.

On the other hand, it has been reported in recent developments in circuit quantum electrodynamics that superconducting devices [including single Cooper pair boxes, Josephson junctions, and superconducting quantum interference devices (SQUIDs)] have a natural superiority for their scalability and are regarded as very prospective candidates to implement QIP [74–88]. Superconducting qubits are relatively easy to scale up and have a long decoherence time [88–90]. Moreover, using SQUID qubits in cavity QED has several advantages. For example, the positions of SQUID qubits in a cavity are fixed while for cavity-atom systems it remains a significant technical challenge to control the center-of-mass motion of a neutral atom [75,76]. Besides, by changing local bias fields or designing suitable variations, the level structure of every individual SQUID qubit can be adjusted readily [75]. Furthermore, when SQUID qubits are embedded in a cavity, the strong-coupling limit of the cavity QED can be easily realized, while for atoms in a cavity, that is difficult to be achieved [76]. Therefore, SQUID qubits are attractive tools for implementing quantum-information tasks.

Combining the advantages of the method with dressed states [59] and SQUID qubits, we investigate the entanglement preparation in the present protocol. Considering the importance of *W* states in both examining quantum nonlocality [91] and implementing quantum-information tasks [92,93], we prepare *W* states for three SQUID qubits by using dressed states as an example. In this protocol, laser pulses can be designed so that a *W* state of three SQUID qubits can be obtained with high speed without using any additional couplings. Besides, the Rabi frequencies of pulses designed by the method with dressed states could be realized without challenges in experiments since they can be expressed by the linear superpositions of Gaussian functions. By selecting suitable control parameters, the populations of the intermediate states can be restrained; hence, the system will suffer less from dissipation of intermediate states. Numerical simulations demonstrate that the protocol is robust against parameter variations and decoherence mechanisms. Different from the protocol for generating *W* states with the adiabatic passages in Ref. [94], in this paper, through choosing a set of suitable dressed states, the protocol can be used to accelerate the adiabatic passages while additional couplings are unnecessary. So, the *W* state can be generated faster than that in Ref. [94].

On the other hand, limited by the adiabatic condition, the *W* state generation in Ref. [94] is more sensitive to dephasing. On the contrary, since the *W* state can be generated fast here, the present protocol is much more robust against dephasing. Therefore, the present protocol is more feasible for experimental realization.

The article is organized as follows. In Sec. II, we review the method to accelerate the adiabatic passages by using dressed states proposed in Ref. [59]. In Sec. III, we describe how to prepare a *W* state of three SQUID qubits by using dressed states. In Sec. IV, we investigate the performance of the protocol via numerical simulations. And finally, the conclusion is given in Sec. V.

II. ACCELERATING THE ADIABATIC PASSAGES BY USING DRESSED STATES

In this section, we would like to review the method to accelerate the adiabatic passages by using dressed states proposed in Ref. [59]. First, we define a picture transformation $U(t) = \sum_n |\varphi_n(t)\rangle\langle n|$, where $\{|\varphi_n(t)\rangle\}$ are the instantaneous eigenstates of the original Hamiltonian $H_0(t)$ corresponding to the eigenvalues $\{E_n(t)\}$, and $\{|n\rangle\}$ is a set of time-independent states. In the adiabatic picture, the Hamiltonian becomes

$$
\begin{aligned}
H_{\mathrm{ad}}(t) &= U^\dagger(t)H_0(t)U(t) + W(t) \\
&= \sum_n E_n(t)|n\rangle\langle n| - iU^\dagger(t)\dot{U}(t),
\end{aligned}
\tag{1}
$$

in which $W(t) = -iU^\dagger(t)\dot{U}(t)$ generically has off-diagonal matrix elements connecting the various instantaneous eigenstates of $H_0(t)$ and causing nonadiabatic errors. In order to correct the nonadiabatic errors, a correction Hamiltonian $H_{\mathrm{co}}(t)$ is introduced such that the modified Hamiltonian $H'(t) = H_0(t) + H_{\mathrm{co}}(t)$. Therefore, in the adiabatic picture, the modified Hamiltonian becomes

$$
\begin{aligned}
H'_{\mathrm{ad}}(t) &= U^\dagger(t)H_0(t)U(t) + U^\dagger(t)H_{\mathrm{co}}(t)U(t) + W(t) \\
&= \sum_n E_n(t)|n\rangle\langle n| + U^\dagger(t)H_{\mathrm{co}}(t)U(t) - iU^\dagger(t)\dot{U}(t) \\
&= H_{\mathrm{ad}}(t) + U^\dagger(t)H_{\mathrm{co}}(t)U(t).
\end{aligned}
\tag{2}
$$

Second, we define another picture transformation $V(t) = \sum_n |\tilde{\varphi}_n(t)\rangle\langle n|$, where $\{|\tilde{\varphi}_n(t)\rangle\}$ is a set of dressed states. Assuming that the initial time is t_i and the final time is t_f, the unitary operator $V(t)$ should satisfy the condition $V(t_i) = V(t_f) = 1$. Then, we move from the adiabatic picture to the new picture called the dressed-state picture. $H'_{\mathrm{ad}}(t)$ in the adiabatic picture becomes

$$
\begin{aligned}
H'_V(t) &= V^\dagger(t)H_{\mathrm{ad}}(t)V(t) + V^\dagger(t)U^\dagger(t)H_{\mathrm{co}}(t)U(t)V(t) \\
&\quad - iV^\dagger(t)\dot{V}(t).
\end{aligned}
\tag{3}
$$

Afterwards, $H_{\mathrm{co}}(t)$ should be carefully designed so that the modified Hamiltonian H'_V and the dressed states $\{|\tilde{\varphi}_n(t)\rangle\}$ satisfy $\langle\tilde{\varphi}_m(t)|H'_V(t)|\tilde{\varphi}_n(t)\rangle = 0 (m \neq n)$; i.e., $H_{\mathrm{co}}(t)$ has to be designed for canceling the unwanted off-diagonal elements in $H_V(t)$.
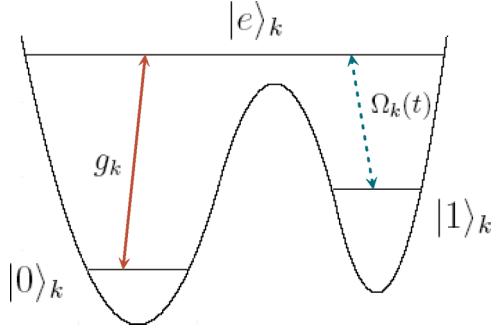
FIG. 1. The level configuration for SQUID$_k$ ($k = 1,2,3,4$).

III. FAST PREPARATION OF *W* STATES FOR THREE SQUID QUBITS BY USING DRESSED STATES

Let us investigate the entanglement preparation with SQUID qubits by using dressed states. As an example, we expound on how to prepare *W* states of three SQUID qubits by using dressed states. The SQUID qubits considered here are rf SQUID qubits. Each SQUID qubit consists of a Josephson tunnel junction in a superconducting loop. The Hamiltonian of each rf SQUID qubit can be described as [75,76]

$$H_s(t) = \frac{Q^2}{2C} + \frac{(\Phi - \Phi_x)^2}{2L} - E_J \cos\left(2\pi \frac{\Phi}{\Phi_0}\right), \quad (4)$$

in which C is the junction capacitance and L is the loop inductance, Q is the total charge on the capacitor, Φ is the magnetic flux threading the loop, Φ_x is the external flux applied to the ring, $\Phi_0 = h/2e$ is the flux quantum, and $E_J = I_c \Phi_0/2\pi$ is the Josephson energy with I_c being the critical current of the junction. We consider that there are four SQUID qubits, SQUID$_1$, SQUID$_2$, SQUID$_3$ and SQUID$_4$, coupled to a single-mode microwave cavity field. As shown in Fig. 1, SQUID$_k$ ($k = 1,2,3,4$) has formed the Λ-type configuration, that is, an excited level $|e\rangle_k$ and two lowest levels $|0\rangle_k$ and $|1\rangle_k$. The classical field with Rabi frequency $\Omega_k(t)$ drives the transition resonantly between the levels $|e\rangle_k$ and $|1\rangle_k$, while the cavity field couples resonantly to the levels $|0\rangle_k$ and $|e\rangle_k$ with coupling constant g_k. $\Omega_k(t)$ and g_k are given in Refs. [75,76] as

$$g_k = \frac{1}{L_k}\sqrt{\frac{\omega_c}{2\mu_0\hbar}}\langle 0|\Phi|e\rangle_k \int_{S_k} \mathbf{B}_c^k(\mathbf{r}) \cdot d\mathbf{S},$$

$$\Omega_k(t) = \frac{1}{2L_k\hbar}\langle 1|\Phi|e\rangle_k \int_{S_k} \mathbf{B}_{\mu w}^k(\mathbf{r},t) \cdot d\mathbf{S}, \quad (5)$$

where S_k is the surface bounded by the loop of SQUID$_k$, L_k is the loop inductance of SQUID$_k$, ω_c is the cavity frequency, and $\mathbf{B}_c^k(\mathbf{r})$ and $\mathbf{B}_{\mu w}^k(\mathbf{r},t)$ are the magnetic components of the cavity mode and the classical microwave in the superconducting loop of SQUID$_k$. The Hamiltonian of the system in the interaction picture with the rotating-wave approximation can be described as ($\hbar = 1$)

$$H_I(t) = H_c + H_m(t), \quad H_c = \sum_{k=1}^{4} g_k|e\rangle_k\langle 0|a + \text{H.c.},$$

$$H_m(t) = \sum_{k=1}^{4} \Omega_k(t)|e\rangle_k\langle 1| + \text{H.c.}, \quad (6)$$

in which a denotes photon the annihilation operator of the cavity mode. For simplicity, we set $g_1 = g_2 = g_3 = g$ and $g_4 = \sqrt{3}g$, which can be realized by adjusting the location or parameters of SQUID$_k$ (e.g., L_k and S_k). Moreover, we assume the system is initially in the state $|\Psi(0)\rangle = |0\rangle_1|0\rangle_2|0\rangle_3|1\rangle_4|0\rangle_c$ ($|0\rangle_c$ and $|1\rangle_c$ are the vacuum state and one-photon state of the cavity mode, respectively). Defining the excited number operator of the system as $N_e = \sum_k(|e\rangle_k\langle e| + |1\rangle_k\langle 1|) + a^\dagger a$, one can obtain that $[N_e, H_I] = 0$ and $\langle\Psi(0)|N_e|\Psi(0)\rangle = 1$. Therefore, the evolution of the system will stay in the one-excited subsystem spanned by

$$\begin{aligned}
|\psi_1\rangle &= |0\rangle_1|0\rangle_2|0\rangle_3|1\rangle_4|0\rangle_c, \\
|\psi_2\rangle &= |0\rangle_1|0\rangle_2|0\rangle_3|e\rangle_4|0\rangle_c, \\
|\psi_3\rangle &= |0\rangle_1|0\rangle_2|0\rangle_3|0\rangle_4|1\rangle_c, \\
|\psi_4\rangle &= |e\rangle_1|0\rangle_2|0\rangle_3|0\rangle_4|0\rangle_c, \\
|\psi_5\rangle &= |0\rangle_1|e\rangle_2|0\rangle_3|0\rangle_4|0\rangle_c, \quad (7) \\
|\psi_6\rangle &= |0\rangle_1|0\rangle_2|e\rangle_3|0\rangle_4|0\rangle_c, \\
|\psi_7\rangle &= |1\rangle_1|0\rangle_2|0\rangle_3|0\rangle_4|0\rangle_c, \\
|\psi_8\rangle &= |0\rangle_1|1\rangle_2|0\rangle_3|0\rangle_4|0\rangle_c, \\
|\psi_9\rangle &= |0\rangle_1|0\rangle_2|1\rangle_3|0\rangle_4|0\rangle_c.
\end{aligned}$$

Here, we would like to prepare the *W* state $|W\rangle = \frac{1}{\sqrt{3}}(|\phi_7\rangle + |\phi_8\rangle + |\phi_9\rangle)$ of SQUID$_1$, SQUID$_2$ and SQUID$_3$. SQUID$_4$ is used to provide a photon to the cavity. Then, we rewrite H_c in this one-excited subspace as $H_c = \sqrt{3}g|\psi_2\rangle\langle\psi_3| + g(|\psi_4\rangle + |\psi_5\rangle + |\psi_6\rangle)\langle\psi_3| + \text{H.c.}$ Assuming $|\varsigma\rangle = \frac{1}{\sqrt{3}}(|\psi_4\rangle + |\psi_5\rangle + |\psi_6\rangle)$, we have $H_c = \sqrt{3}g|\psi_1\rangle\langle\psi_2| + \sqrt{3}g|\varsigma\rangle\langle\psi_2| + \text{H.c.}$ The eigenstates of H_c are calculated in the following:

$$|\phi_0\rangle = \frac{1}{\sqrt{2}}(-|\psi_2\rangle + |\varsigma\rangle),$$

$$|\phi_1\rangle = \frac{1}{2}(|\psi_2\rangle + \sqrt{2}|\psi_3\rangle + |\varsigma\rangle), \quad (8)$$

$$|\phi_2\rangle = \frac{1}{2}(|\psi_2\rangle - \sqrt{2}|\psi_3\rangle + |\varsigma\rangle),$$

with eigenvalues $E_0 = 0$, $E_1 = \sqrt{6}g$, and $E_3 = -\sqrt{6}g$, respectively. For simplicity, we assume that $\Omega_1(t) = \Omega_2(t) = \Omega_3(t) = \sqrt{2}\Omega_a(t)$ and $\Omega_4(t) = \sqrt{2}\Omega_b(t)$. By adding the condition $\Omega_a, \Omega_b \ll g$, the effective Hamiltonian of the system can be given by

$$\begin{aligned}
H_{\text{eff}}(t) &= \frac{\Omega_a(t)}{\sqrt{3}}(|\psi_7\rangle + |\psi_8\rangle + |\psi_9\rangle)\langle\phi_0| \\
&\quad - \Omega_b(t)|\psi_1\rangle\langle\phi_0| + \text{H.c.} \\
&= \Omega_a(t)|W\rangle\langle\phi_0| - \Omega_b(t)|\psi_1\rangle\langle\phi_0| + \text{H.c.} \quad (9)
\end{aligned}$$

Assuming $\Omega_a(t) = \Omega(t)\cos\theta(t)$ and $\Omega_b(t) = \Omega(t)\sin\theta(t)$, the three instantaneous eigenstates of $H_{\text{eff}}(t)$ can be described as

$$|\varphi_0(t)\rangle = \cos\theta|\psi_1\rangle + \sin\theta|W\rangle,$$

$$|\varphi_+(t)\rangle = \frac{1}{\sqrt{2}}(\sin\theta|\psi_1\rangle + |\phi_0\rangle - \cos\theta|W\rangle), \quad (10)$$

$$|\varphi_-(t)\rangle = \frac{1}{\sqrt{2}}(\sin\theta|\psi_1\rangle - |\phi_0\rangle - \cos\theta|W\rangle),$$

with eigenvalues $\epsilon_0 = 0$, $\epsilon_+(t) = \Omega(t)$, and $\epsilon_-(t) = -\Omega(t)$, respectively. A general adiabatic state transfer from the initial state $|\psi_1\rangle$ to the target state $|W\rangle$ can be performed via $|\varphi_0(t)\rangle$ with boundary condition $\theta(0) = 0$ and $\theta(T) = \pi/2$. To speed up the evolution using dressed states, we first go into the adiabatic picture. By using picture transformation $U(t) = \sum_{n=0,+,-} |\varphi_n(t)\rangle\langle n|$, the Hamiltonian in the adiabatic picture is

$$H_{\text{ad}}(t) = \Omega(t)M_z + \dot{\theta}(t)M_y, \tag{11}$$

where

$$M_x = \frac{1}{\sqrt{2}}\begin{bmatrix} 0 & -1 & 1 \\ -1 & 0 & 0 \\ 1 & 0 & 0 \end{bmatrix},$$

$$M_y = \frac{1}{\sqrt{2}}\begin{bmatrix} 0 & -i & -i \\ i & 0 & 0 \\ i & 0 & 0 \end{bmatrix}, \tag{12}$$

$$M_z = \begin{bmatrix} 0 & 0 & 0 \\ 0 & 1 & 0 \\ 0 & 0 & -1 \end{bmatrix}$$

are spin-1 operators, obeying the commutation relation $[M_p, M_q] = i\varepsilon^{pqr}M_r$ with the Levi-Civita symbol ε^{pqr}.

As shown in Ref. [59], moving to a dressed-state picture, one can choose a picture transformation

$$V(t) = \exp[i\eta(t)M_z]\exp[i\mu(t)M_x]\exp[i\xi(t)M_z], \tag{13}$$

which is parametrized as a rotation of spin with Euler angles $\xi(t)$, $\mu(t)$, and $\eta(t)$. Moreover, to fulfill the condition $V(0) = V(T) = 1$, the angle $\mu(t)$ should satisfy $\mu(0) = \mu(T) = 0(2\pi)$, and the other two angles can have arbitrary values. If we want the correction Hamiltonian $H_{\text{co}}(t)$ to have the same form as $H_{\text{eff}}(t)$, $H_{\text{co}}(t)$ can be chosen to have the general form

$$H_{\text{co}}(t) = U(t)(g_x(t)M_x + g_z(t)M_z)U^\dagger(t), \tag{14}$$

where $g_x(t)$ and $g_z(t)$ are two control parameters. Therefore, what we need is only a simple modification of the original angle $\theta(t)$ and amplitude $\Omega(t)$ as

$$\theta(t) \to \tilde{\theta}(t) = \theta(t) - \arctan\left(\frac{g_x(t)}{\Omega(t) + g_z(t)}\right),$$

$$\Omega(t) \to \tilde{\Omega}(t) = \sqrt{[\Omega(t) + g_z(t)]^2 + g_x^2(t)}. \tag{15}$$

In addition, to cancel the unwanted transitions between dressed states in the dressed-state picture, the control parameters should be chosen as

$$g_x(t) = \frac{\dot{\mu}}{\cos\xi} - \dot{\theta}\tan\xi,$$

$$g_z(t) = -\Omega + \dot{\xi} + \frac{\dot{\mu}\sin\xi - \dot{\theta}}{\tan\mu\cos\xi}, \tag{16}$$

and they are independent of $\eta(t)$. Moreover, the population of the intermediate state $|\phi_0\rangle$ is given by

$$|\langle\Psi(t)|\phi_0(t)\rangle| = \sin^2\mu(t)\cos^2\xi(t). \tag{17}$$

For simplicity, we choose $\xi(t) \equiv 0$. To fulfill the boundary conditions $\mu(0) = \mu(T) = 0(2\pi)$, $\theta(0) = 0$, and $\theta(T) = \pi/2$

as well as avoid the singularity of the expression for each pulse, we adopt the following parameters:

$$\theta(t) = \frac{\pi t}{2T} - \frac{1}{3}\sin\left(\frac{2\pi t}{T}\right) + \frac{1}{24}\sin\left(\frac{4\pi t}{T}\right),$$

$$\dot{\theta}(t) = \frac{4\pi}{3T}\sin^4\left(\frac{\pi t}{T}\right),$$

$$\mu(t) = \frac{A}{2}\left[1 - \cos\left(\frac{2\pi t}{T}\right)\right],$$

$$\dot{\mu}(t) = \frac{\pi A}{T}\sin\left(\frac{2\pi t}{T}\right), \tag{18}$$

where A is a time-independent parameter which controls the maximal value of $\mu(t)$. If we set $0 < A < \pi/2$, when A decreases, the population of intermediate state $|\phi_0\rangle$ also decreases. However, according to the expression of $g_z(t)$, the value of $\tilde{\Omega}(t) \times T$ will increase; that means one has to increase the interaction time T when the pulses' amplitude $\tilde{\Omega}(t)$ has a fixed value. Therefore, it is better to choose a suitable A, so that both the population of intermediate state $|\phi_0\rangle$ and the interaction time can be restricted in a desired range. We find that $A = 0.5$ can meet our requirement, which gives $|\langle\Psi(t)|\phi_0(t)\rangle| = \sin^2\mu(t) \leqslant 0.23$ and $\tilde{\Omega}(t) \times T \approx 7$. Until now, the question still remains whether the expressions of pulses $\tilde{\Omega}_a(t) = \tilde{\Omega}(t)\cos\tilde{\theta}(t)$ and $\tilde{\Omega}_b(t) = \tilde{\Omega}(t)\sin\tilde{\theta}(t)$ are too complex for realization in experiments. In order to make the protocol more feasible in experiments, the Rabi frequencies of pulses should be expressed by some frequently used functions, e.g., Gaussian functions and sine functions, or their linear superpositions. Thanks to the curve fitting, we find two replaceable pulses $\bar{\Omega}_a(t)$ and $\bar{\Omega}_b(t)$ for $\tilde{\Omega}_a(t)$ and $\tilde{\Omega}_b(t)$, respectively, as

$$\bar{\Omega}_a(t) = \zeta_{a_1}e^{-[(t-\tau_{a_1})/\chi_{a_1}]^2} + \zeta_{a_2}e^{-[(t-\tau_{a_2})/\chi_{a_2}]^2},$$

$$\bar{\Omega}_b(t) = \zeta_{b_1}e^{-[(t-\tau_{b_1})/\chi_{b_1}]^2} + \zeta_{b_2}e^{-[(t-\tau_{b_2})/\chi_{b_2}]^2}, \tag{19}$$

where

$$\zeta_{a_1} = 6.226/T, \quad \zeta_{a_2} = 1.332/T,$$
$$\zeta_{b_1} = 6.226/T, \quad \zeta_{b_2} = 1.332/T,$$
$$\tau_{a_1} = 0.597T, \quad \tau_{a_2} = 0.2395T,$$
$$\tau_{b_1} = 0.4033T, \quad \tau_{b_2} = 0.7605T,$$
$$\chi_{a_1} = 0.2214T, \quad \chi_{a_2} = 0.1971T,$$
$$\chi_{b_1} = 0.2214T, \quad \chi_{b_2} = 0.1971T. \tag{20}$$

Here, ζ_{α_β} ($\alpha = a,b, \beta = 1,2$) is the pulse amplitude of the βth component in pulse $\Omega_\alpha(t)$, τ_{α_β} describes the extreme point of the βth component in pulse $\Omega_\alpha(t)$, and χ_{α_β} controls the width of the βth component in pulse $\Omega_\alpha(t)$. As a comparison, we plot $\tilde{\Omega}_a(t)$ [$\tilde{\Omega}_b(t)$] with $\bar{\Omega}_a(t)$ [$\bar{\Omega}_b(t)$] versus t/T in Fig. 2(a) [Fig. 2(b)]. As shown in Fig. 2, the solid blue curve for $\bar{\Omega}_a(t)$ [$\bar{\Omega}_b(t)$] and the dashed red curve for $\tilde{\Omega}_a(t)$ [$\tilde{\Omega}_b(t)$] are considerably close to each other. In the next section, pulses with Rabi frequencies $\bar{\Omega}_1(t) = \sqrt{2}\bar{\Omega}_a(t)$, $\bar{\Omega}_2(t) = \sqrt{2}\bar{\Omega}_a(t)$, $\bar{\Omega}_3(t) = \sqrt{2}\bar{\Omega}_a(t)$, and $\bar{\Omega}_4(t) = \sqrt{2}\bar{\Omega}_b(t)$ are demonstrated to drive the system from its initial state $|\Psi(0)\rangle = |\psi_1\rangle$ to the target state $|\Psi(T)\rangle = |W\rangle$ with high fidelity via numerical
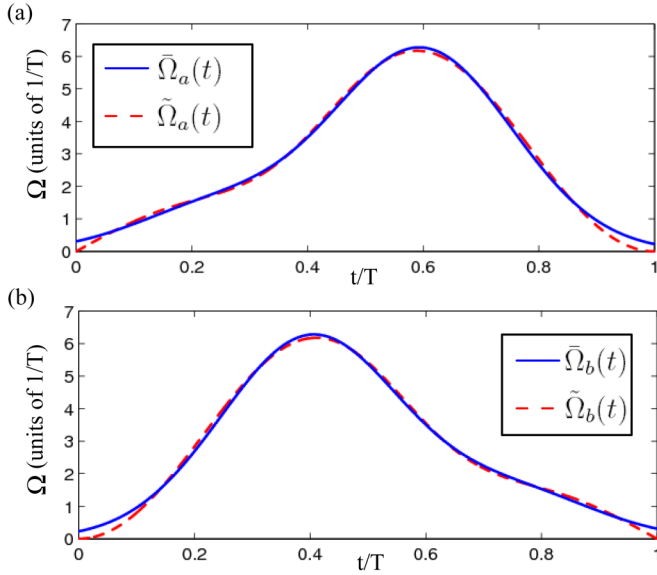
(a)

(b)

FIG. 2. (a) Comparison between $\tilde{\Omega}_a(t)$ (dashed red line) and $\bar{\Omega}_a(t)$ (solid blue line) (versus t/T). (b) Comparison between $\tilde{\Omega}_b(t)$ (dashed red line) and $\bar{\Omega}_b(t)$ (solid blue line) (versus t/T).

simulations for the sake of proving that the replacements here for the Rabi frequencies of the pulses are effective.

IV. NUMERICAL SIMULATIONS

In this section, we investigate the performance of the protocol via numerical simulations. The fidelity of the target state $|W\rangle$ is defined as $F(t) = |\langle W|\rho(t)|W\rangle|$, where $\rho(t)$ is the density operator of the system. First, as a condition $\Omega_a, \Omega_b \ll g$ is set to obtain the effective Hamiltonian $H_{\text{eff}}(t)$, so before doing numerical simulations and further discussions based on the original Hamiltonian $H_I(t)$ in the interaction picture, we need to choose a suitable value for coupling constant g. In the present protocol, the pulse amplitude is $\bar{\Omega}_0 = \max_{0 \leqslant t \leqslant T_{k=1,2,3,4}}\{\bar{\Omega}_k(t)\} \approx 9.8/T$, and the condition $\Omega_a, \Omega_b \ll g$ can be replaced by $\bar{\Omega}_0 \ll g$. Seen from Fig. 3, the final fidelity $F(T)$ is almost 1 when $g \geqslant 10/T$. That means even if the condition $\bar{\Omega}_0 \ll g$ is violated, one can also obtain a W state by using the present protocol. Generally speaking, since the coupling constant g has an upper limit in real experiments, the condition $\bar{\Omega}_0 \ll g$ may cause the speed limit of the system's evolution. But when $\bar{\Omega}_0 \ll g$ is fulfilled, the system is guided by the effective Hamiltonian $H_{\text{eff}}(t)$, so the
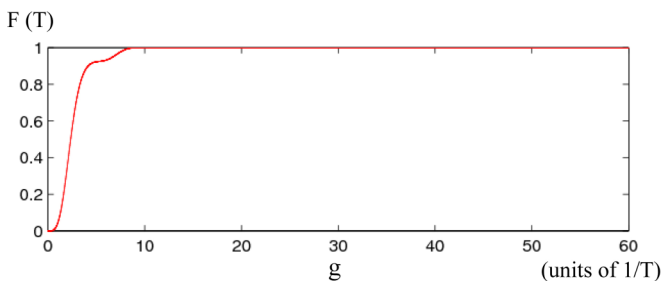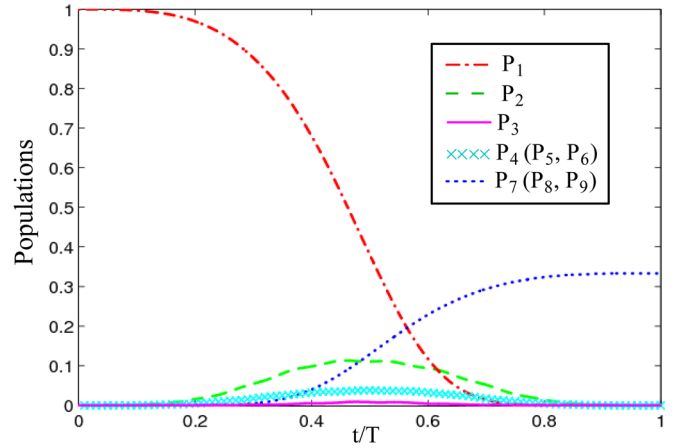

FIG. 3. The final fidelity $F(T)$ versus g.

FIG. 4. The population P_ι ($\iota = 1,2,3,\ldots,9$) of state $|\psi_\iota\rangle$ versus t/T: P_1, dash-dotted red line; P_2, dashed green line; P_3, solid pink line; P_4, P_5, and P_6, light blue crosses; and P_7, P_8, and P_9, dotted blue line.

dark state $|\phi_0\rangle$ of H_c has an absolute predominance among all the intermediate states. Since $|\phi_0\rangle$ has a lower energy compared with other eigenstates of H_c, using $|\phi_0\rangle$ as the intermediate state while restraining populations for other eigenstates of H_c can help us to reduce the dissipation. However, when g is not large enough, the system will evolve along an unknown path, which is not decided by the effective Hamiltonian. As a result, the population of each intermediate state cannot be forecasted as before; meanwhile, $|\phi_0\rangle$ does not predominate in this case. Thus, dissipation will increase, finally resulting in a relatively bad performance when decoherence mechanisms are taken into account. Therefore, for both high speed and robustness against dissipation, we adopt $g = 30/T$, slightly larger than $\bar{\Omega}_0$ ($\bar{\Omega}_0/g \approx 0.33$). After the coupling constant g is chosen, we would like to examine the population $P_\iota = \langle\psi_\iota|\rho(t)|\psi_\iota\rangle$ ($\iota = 1,2,\ldots,9$) of state $|\psi_\iota\rangle$ during the evolution. So, we plot P_ι versus t/T in Fig. 4. As shown in Fig. 4, the population $|\psi_3\rangle$ (see the solid pink line of Fig. 4), which is not the component of $|\phi_0\rangle$, stays nearly zero during the evolution. This result coincides with the dynamics governed by $H_{\text{eff}}(t)$. Finally at $t = T$, the target state $|W\rangle$ can be obtained.

Second, since accelerating the adiabatic passage is the purpose of implementing the present protocol, it is necessary to show the present protocol is faster than preparing a W state with adiabatic passages. Here, considering STIRAP is a famous method for adiabatic passages, we start by constructing an adiabatic passage to prepare a W state using STIRAP. We can design the Rabi frequencies of pulses as

$$\Omega_1'(t) = \Omega_2'(t) = \Omega_3'(t) = \Omega_0' e^{-[(t-t_0-T/2)/t_c]^2},$$
$$\Omega_4'(t) = \Omega_0' e^{-[(t+t_0-T/2)/t_c]^2}, \quad (21)$$

where Ω_0' is the pulse amplitude for STIRAP, and $t_0 = 0.15T$ and $t_c = 0.2T$ are two related parameters. Then, to compare the present protocol with that of STIRAP, we plot Fig. 5 to show the fidelities of obtaining the target state $|W\rangle$ versus t/T with different methods. As shown in Fig. 5, the fidelity of the
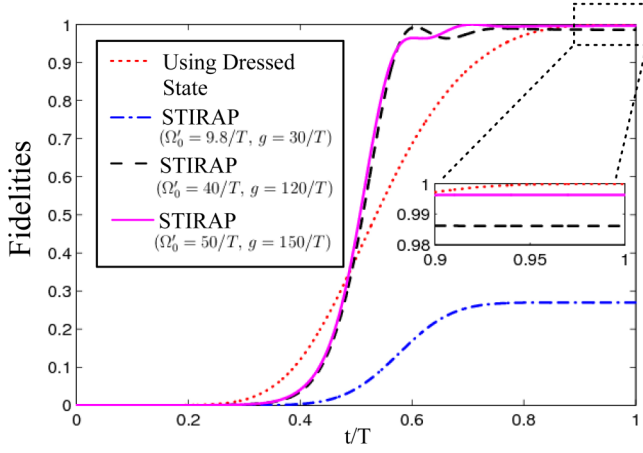
FIG. 5. The fidelities of the target state $|W\rangle$ versus t/T with different methods: dotted red line, using the dressed method; dash-dotted blue line, STIRAP with $\Omega_0 = 9.8/T$ and $g = 30/T$; dashed black line, STIRAP with $\Omega_0 = 40/T$ and $g = 120/T$; and solid pink line, STIRAP with $\Omega_0 = 50/T$ and $g = 150/T$.

present protocol can reach 1 at $t = T$ (see the dotted red line in Fig. 5) while with the same condition for STIRAP ($\Omega'_0 = 9.8/T$, $g = 30/T$; see the dash-dotted blue line in Fig. 5), the fidelity is only about 0.275 due to the bad violation of the adiabatic condition. So we increase the pulse amplitude Ω'_0 and the coupling constant g to $40/T$ and $120/T$, respectively. In this case (see the dashed black line in Fig. 5), the fidelity can increase close to 1; however, the final fidelity is only 0.985, still a little disappointing. Finally, when the pulse amplitude Ω'_0 is increased to $50/T$, and g is increased to $150/T$, the

fidelity approaches 1 even more (above 0.99); however, its performance is still worse than that of the present protocol (see the solid pink line in Fig. 5). As we mentioned in Sec. III, for a relatively high speed, the product of the pulse amplitude Ω_0 and the total interaction time T is better the smaller it is. Because when Ω_0 takes a fixed value (such as the upper limit for the system), the one that has the smaller product $\Omega_0 T$ will have less interaction time. In the present protocol, the pulse amplitude $\bar{\Omega}_0$ is only $9.8/T$, while for STIRAP, to obtain a high enough fidelity, one should set $\Omega'_0 \geqslant 50/T$. Therefore, the speed of the present protocol to obtain the target state is a lot faster compared with that of STIRAP.

Third, in real experiments, the dissipation caused by decoherence mechanisms are ineluctable. Therefore, we would like to check the fidelity $F(T)$ when decoherence mechanisms are taken into account in order to help us to forecast the experimental feasibility. In the present protocol, the major factors of decoherence mechanisms are (i) cavity decay (with decay rate κ); (ii) the spontaneous emissions from $|e\rangle_k$ to $|0\rangle_k$ and $|1\rangle_k$ with spontaneous emission rates γ_{0k} and γ_{1k}, respectively; and (iii) the dephasing between $|e\rangle_k$ and $|0\rangle_k$ ($|e\rangle_k$ and $|1\rangle_k$) with dephasing rate $\gamma_{\phi0k}$ ($\gamma_{\phi1k}$) ($k = 1,2,3,4$). The evolution of the system can be described by a master equation in Lindblad form as follows:

$$\dot{\rho} = i[\rho, H_I] + \sum_l \left[L_l \rho L_l^\dagger - \frac{1}{2}(L_l^\dagger L_l \rho + \rho L_l^\dagger L_l) \right], \quad (22)$$

where L_l ($l = 1,2,3,\ldots,17$) is the Lindblad operator. There are 17 Lindblad operators in the present protocol:

$$
\begin{aligned}
&L_1 = \sqrt{\gamma_{11}}|1\rangle_1\langle e|, \quad L_2 = \sqrt{\gamma_{12}}|1\rangle_2\langle e|, \quad L_3 = \sqrt{\gamma_{13}}|1\rangle_3\langle e|, \quad L_4 = \sqrt{\gamma_{14}}|1\rangle_4\langle e|, \\
&L_5 = \sqrt{\gamma_{01}}|0\rangle_1\langle e|, \quad L_6 = \sqrt{\gamma_{02}}|0\rangle_2\langle e|, \quad L_7 = \sqrt{\gamma_{03}}|0\rangle_3\langle e|, \quad L_8 = \sqrt{\gamma_{04}}|0\rangle_4\langle e|, \\
&L_9 = \sqrt{\gamma_{\phi11}/2}(|e\rangle_1\langle e| - |1\rangle_1\langle 1|), \quad L_{10} = \sqrt{\gamma_{\phi12}/2}(|e\rangle_2\langle e| - |1\rangle_2\langle 1|), \\
&L_{11} = \sqrt{\gamma_{\phi13}/2}(|e\rangle_3\langle e| - |1\rangle_3\langle 1|), \quad L_{12} = \sqrt{\gamma_{\phi14}/2}(|e\rangle_4\langle e| - |1\rangle_4\langle 1|), \\
&L_{13} = \sqrt{\gamma_{\phi01}/2}(|e\rangle_1\langle e| - |0\rangle_1\langle 0|), \quad L_{14} = \sqrt{\gamma_{\phi02}/2}(|e\rangle_2\langle e| - |0\rangle_2\langle 0|), \\
&L_{15} = \sqrt{\gamma_{\phi03}/2}(|e\rangle_3\langle e| - |0\rangle_3\langle 0|), \quad L_{16} = \sqrt{\gamma_{\phi04}/2}(|e\rangle_4\langle e| - |0\rangle_4\langle 0|), \quad L_{17} = \sqrt{\kappa}a. \quad (23)
\end{aligned}
$$

For simplicity, we assume $\gamma_{1k} = \gamma_{0k} = \gamma$ and $\gamma_{\phi1k} = \gamma_{\phi0k} = \gamma_\phi$ in the following discussions. The final fidelity $F(T)$ versus κ/g and γ/g is given in Fig. 6(a), the final fidelity $F(T)$ versus κ/g and γ_ϕ/g is given in Fig. 6(b), and the final fidelity $F(T)$ versus γ/g and γ_ϕ/g is given in Fig. 6(c). Some samples of the final fidelity $F(T)$ with corresponding κ/g, γ/g, and γ_ϕ/g are given in Table I. According to Fig. 6 and Table I, we have the following results:

(i) $F(T)$ is very robust against the cavity decay since the population of $|\psi_3\rangle$ is restrained (see Fig. 4).

(ii) $F(T)$ is more sensitive to the spontaneous emissions than the cavity decay. However, when γ/g increases from 0 to 0.01, $F(t)$ remains higher than 0.957 with $\gamma_\phi = 0$ and $\kappa = 0$. We can say the present protocol to prepare W states is also robust against the spontaneous emissions.

(iii) The dephasing influences $F(T)$ the most. When γ_ϕ/g increases from zero to only 1×10^{-3}, $F(T)$ falls from 1 to 0.983.

We also investigate the performance of STIRAP when dephasing is taken into account. As a comparison, we plot the final fidelities $F(T)$ versus γ_ϕ/g for both the present protocol (dashed red line) and the STIRAP protocol (solid blue line) in Fig. 7. As shown in Fig. 7, with STIRAP, $F(T)$ decreases from 1 to 0.942 when γ_ϕ/g increases from zero to 1×10^{-3}. Comparing with STIRAP, it is obvious that the present protocol is more robust against dephasing on account of the acceleration for the evolution speed. In addition, Refs. [76,95] have shown that $g \sim 180$ MHz, $\gamma \sim 1.32$ MHz, $\kappa \sim 1.32$ MHz, and $\gamma_\phi \sim 10$ kHz can be realized in real experiments. Submitting these parameters into Eqs. (22)
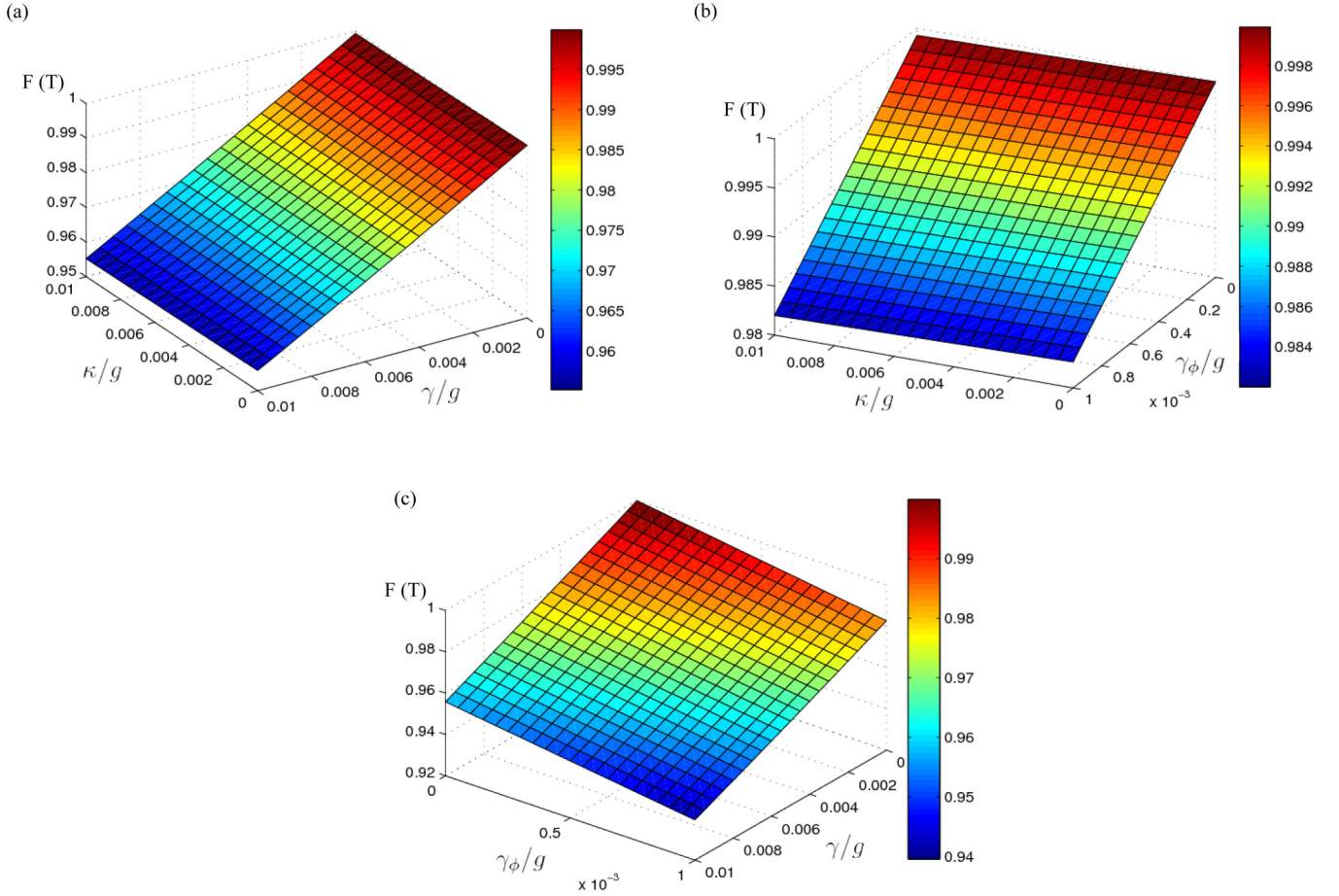
(a)

(b)

(c)

FIG. 6. (a) The final fidelity $F(T)$ versus κ/g and γ/g. (b) The final fidelity $F(T)$ versus κ/g and γ_ϕ/g. (c) The final fidelity $F(T)$ versus γ/g and γ_ϕ/g.

and (23), we have $F(T) = 0.9659$. Therefore, the present protocol could work well when decoherence mechanisms are considered.

TABLE I. Samples of the final fidelity $F(T)$ with corresponding κ/g, γ/g, and γ_ϕ/g.

κ/g ($\times 10^{-2}$)	γ/g ($\times 10^{-2}$)	γ_ϕ/g ($\times 10^{-3}$)	$F(T)$
1	1	1	0.9389
1	1	0.8	0.9421
1	0.8	1	0.9473
0.8	1	1	0.9390
0.8	0.8	0.8	0.9507
0.8	0.8	0.5	0.9556
0.8	0.5	0.8	0.9635
0.5	0.8	0.8	0.9509
0.5	0.5	0.5	0.9687
0.5	0.5	0.3	0.9721
0.5	0.3	0.5	0.9775
0.3	0.5	0.5	0.9659
0.3	0.3	0.3	0.9811
0.3	0.3	0.1	0.9845
0.3	0.1	0.3	0.9900
0.1	0.3	0.3	0.9812
0.1	0.1	0.1	0.9936

Fourth, due to the variations of the parameters caused by the experimental imperfection operations, the evolution of the system will deviate from our expectation. It is worthwhile to investigate the influences from variations of the parameters caused by the experimental imperfection. Here we would like to discuss the variations δT, $\delta \bar{\Omega}_0$, and δg of the total evolution time T, pulse amplitude $\bar{\Omega}_0$, and the coupling constant g, respectively. We assume that $T' = T + \delta T$ is the erroneous total interaction time when there is a variation δT for the original interaction time. We plot $F(T')$ versus $\delta T/T$ and $\delta g/g$ in Fig. 8(a), $F(T')$ versus $\delta T/T$ and $\delta \bar{\Omega}_0/\bar{\Omega}_0$ in Fig. 8(b), and
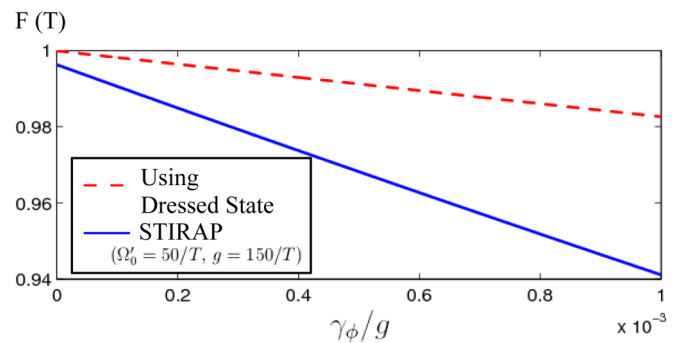

FIG. 7. The final fidelities $F(T)$ versus γ_ϕ/g for the present protocol (dashed red line) and that with STIRAP (solid blue line).
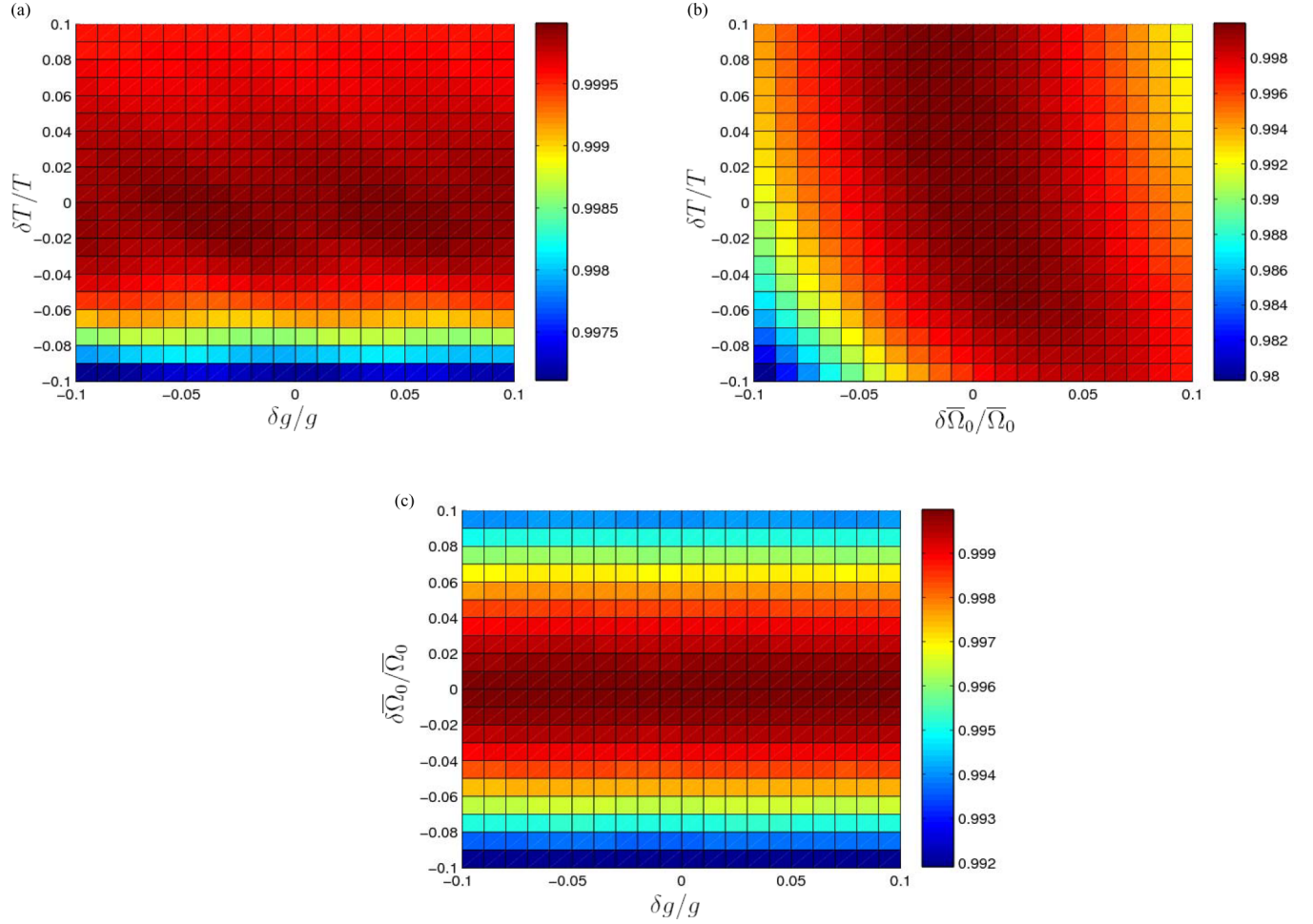
FIG. 8. (a) The final fidelity $F(T')$ versus $\delta T/T$ and $\delta g/g$. (b) The final fidelity $F(T')$ versus $\delta T/T$ and $\delta\bar{\Omega}_0/\bar{\Omega}_0$. (c) The final fidelity $F(T)$ versus $\delta\bar{\Omega}_0/\bar{\Omega}_0$ and $\delta g/g$.

$F(T)$ versus $\delta g/g$ and $\delta\bar{\Omega}_0/\bar{\Omega}_0$ in Fig. 8(c). Some samples of the final fidelity $F(T')$ with corresponding $\delta T/T$, $\delta\bar{\Omega}_0/\bar{\Omega}_0$, and $\delta g/g$ are given in Table II. According to Fig. 8 and Table II, we can obtain the following results:

(i) Seen from Fig. 8(a), $F(T')$ is insensitive to the variation δg for the coupling strength. Besides, Fig. 8(c) shows that $F(T)$ is almost not influenced by the variation δg. This result is because we have chosen a suitable coupling constant $g = 30/T$ in the first part of the discussions. It is also shown in Fig. 3 that the final fidelity is nearly 1 when $g \geqslant 10/T$. Therefore, the coupling constant we chose is good enough to resist the variation δg.

(ii) As shown in Figs. 8(a) and 8(b), $F(T')$ is also very robust to the variation δT of the total interaction time. When $T' = 0.9T$ with $\delta g = 0$ and $\delta\bar{\Omega}_0 = 0$, the fidelity only decreases about 0.003. Moreover, when $T' > T$, the fidelity is almost unchanged and close to 1, on account of the suitable boundary condition for control parameters (e.g., θ, $\dot{\theta}$, μ, and $\dot{\mu}$) set in Sec. III.

(iii) The variation $\delta\bar{\Omega}_0$ of pulse amplitude $\bar{\Omega}_0$ influences the fidelity mostly according to Figs. 8(b) and 8(c). However, as shown in Fig. 8(b), $F(T')$ is still higher than 0.98 even when $|\delta\bar{\Omega}_0/\bar{\Omega}_0| = |\delta T/T| = 10\%$, and as shown

in Fig. 8(c), $F(T')$ is still higher than 0.992 even when $|\delta\bar{\Omega}_0/\bar{\Omega}_0| = |\delta g/g| = 10\%$. This indicates that the present protocol holds robustness against the variation $\delta\bar{\Omega}_0$ as well.

(iv) There is an interesting phenomenon shown in Fig. 8(b); i.e., when $\delta\bar{\Omega}_0$ and δT have the same sign (both positive or both negative), the fidelity remains at a high level. This tells us that if we have smaller (larger) pulse amplitudes than the designed one, we should increase (reduce) interaction time to correct the error.

TABLE II. Samples of the final fidelity $F(T')$ with corresponding $\delta T/T$, $\delta\bar{\Omega}_0/\bar{\Omega}_0$, and $\delta g/g$.

$\delta T/T$	$\delta\bar{\Omega}_0/\bar{\Omega}_0$	$\delta g/g$	$F(T')$
10%	10%	10%	0.9907
10%	10%	−10%	0.9907
10%	−10%	10%	0.9944
10%	−10%	−10%	0.9944
−10%	10%	10%	0.9965
−10%	10%	−10%	0.9964
−10%	−10%	10%	0.9798
−10%	−10%	−10%	0.9796

Based on the discussions above, we conclude that the present protocol is robust against the variations δT, $\delta \bar{\Omega}_0$, and δg.

V. CONCLUSION

In conclusion, we have proposed a protocol to prepare *W* states with SQUID qubits by using dressed states. First, we examined and simplified the system's dynamics and obtained the effective Hamiltonian so that the simplified model can be regarded as a three-level system. This greatly helps us to further investigate the speeding up of the system's evolution with dressed states. Second, we applied the method with dressed states to the simplified three-level model, in order to keep the system evolving along a suitable dressed state during the evolution. And we carefully designed the parameters θ, $\dot{\theta}$, μ, and $\dot{\mu}$, which are shown in Eq. (18). With these parameters, the Rabi frequencies of pulses being designed can be expressed by the superpositions of Gaussian functions with curve fitting, so that they are feasible for experimental realization. Third, we selected a suitable coupling constant g for both robustness and speediness. With the designed pulses and the chosen coupling constant, we continued to explore the robustness against all kinds of influencing factors, including the cavity decay, the spontaneous emissions of SQUID qubits, the dephasing, and some parameter variations caused by the imperfect operations, and we found that the present protocol holds great robustness against these influencing factors. Meanwhile, we compared the evolution speed of the present protocol with that of STIRAP. The results showed that the evolution speed of the present protocol is much faster than that of STIRAP. On the other hand, in experiment, the SQUID qubits have a lot of advantages as we discussed in Sec. I. Therefore, we hope the present protocol can be realized in circuit quantum electrodynamics systems and contribute to the quantum-information processing in the near future.

[1] J. Lee, M. Paternostro, M. S. Kim, and S. Bose, Phys. Rev. Lett. **96**, 080501 (2006).

[2] C. P. Yang, Phys. Rev. A **82**, 054303 (2010).

[3] M. Amniat-Talab, S. Guérin, N. Sangouard, and H. R. Jauslin, Phys. Rev. A **71**, 023805 (2005).

[4] M. Saffman, T. G. Walker, and K. Mølmer, Rev. Mod. Phys. **82**, 2313 (2010).

[5] A. Ruschhaupt and J. G. Muga, Phys. Rev. A **73**, 013608 (2006).

[6] F. P. Dos Santos, H. Marion, S. Bize, Y. Sortais, A. Clairon, and C. Salomon, Phys. Rev. Lett. **89**, 233004 (2002).

[7] M. Weitz, B. C. Young, and S. Chu, Phys. Rev. Lett. **73**, 2563 (1994).

[8] P. Král, I. Thanopulos, and M. Shapiro, Rev. Mod. Phys. **79**, 53 (2007).

[9] K. Bergmann, H. Theuer, and B. W. Shore, Rev. Mod. Phys. **70**, 1003 (1998).

[10] M. P. Fewell, B. W. Shore, and K. Bergmann, Aust. J. Phys. **50**, 281 (1997).

[11] N. V. Vitanov, T. Halfmann, B. W. Shore, and K. Bergmann, Annu. Rev. Phys. Chem. **52**, 763 (2001).

[12] X. Wei and M. F. Chen, Quantum Inf. Process. **14**, 2419 (2015).

[13] J. L. Wu, C. Song, J. Xu, L. Yu, X. Ji, and S. Zhang, Quantum Inf. Process. **15**, 3663 (2016).

[14] M. Demirplak and S. A. Rice, J. Phys. Chem. A **107**, 9937 (2003).

[15] M. Demirplak and S. A. Rice, J. Chem. Phys. **129**, 154111 (2008).

[16] E. Torrontegui, S. Ibáñez, S. Martínez-Garaot, M. Modugno, A. del Campo, D. Gué-Odelin, A. Ruschhaupt, X. Chen, and J. G. Muga, Adv. At. Mol. Opt. Phys. **62**, 117 (2013).

[17] J. G. Muga, X. Chen, A. Ruschhaupt, and D. Guéry-Odelin, J. Phys. B **42**, 241001 (2009).

[18] X. Chen, A. Ruschhaupt, S. Schmidt, A. del Campo, D. Guéry-Odelin, and J. G. Muga, Phys. Rev. Lett. **104**, 063002 (2010).

[19] A. del Campo and M. G. Boshier, Sci. Rep. **2**, 648 (2012).

[20] X. Chen, I. Lizuain, A. Ruschhaupt, D. Guéry-Odelin, and J. G. Muga, Phys. Rev. Lett. **105**, 123003 (2010).

[21] A. del Campo, Phys. Rev. Lett. **111**, 100502 (2013).

[22] X. Chen, E. Torrontegui, and J. G. Muga, Phys. Rev. A **83**, 062116 (2011).

[23] M. V. Berry, J. Phys. A **42**, 365303 (2009).

[24] X. K. Song, H. Zhang, Q. Ai, J. Qiu, and F. G. Deng, New J. Phys. **18**, 023001 (2016).

[25] Z. Chen, Y. H. Chen, Y. Xia, J. Song, and B. H. Huang, Sci. Rep. **6**, 22202 (2016).

[26] Y. H. Chen, Y. Xia, J. Song, and Q. Q. Chen, Sci. Rep. **5**, 15616 (2016).

[27] Y. H. Chen, B. H. Huang, J. Song, and Y. Xia, Opt. Commun. **380**, 140 (2016).

[28] X. B. Huang, Z. R. Zhong, and Y. H. Chen, Quantum Inf. Process. **14**, 4475 (2015).

[29] W. J. Shan, Y. Xia, Y. H. Chen, and J. Song, Quantum Inf. Process. **15**, 2359 (2016).

[30] A. C. Santos and M. S. Sarandy, Sci. Rep. **5**, 15775 (2015).

[31] A. C. Santos, R. D. Silva, and M. S. Sarandy, Phys. Rev. A **93**, 012311 (2016).

[32] I. Hen, Phys. Rev. A **91**, 022309 (2015).

[33] M. S. Sarandy, L. A. Wu, and D. Lidar, Quantum Inf. Process. **3**, 331 (2004).

[34] I. B. Coulamy, A. C. Santos, I. Hen, and M. S. Sarandy, Front. ICT **3**, 19 (2016).

[35] M. M. Rams, M. Mohseni, and A. del Campo, arXiv:1606.07740.

[36] S. Deffner, C. Jarzynski, and A. del Campo, Phys. Rev. X **4**, 021013 (2014).

[37] A. del Campo, Shortcuts to adiabaticity in quantum many-body systems: A quantum dynamical micro-

scope, APS March Meeting 2014, Vol. 59, Number 1, http://meetings.aps.org/link/BAPS.2014.MAR.Q34.11.

[38] A. del Campo, Phys. Rev. A **84**, 031606(R) (2011).

[39] A. del Campo, M. M. Rams, and W. H. Zurek, Phys. Rev. Lett. **109**, 115703 (2012).

[40] S. An, D. Lv, A. del Campo, and K. Kim, Nat. Commun. **7**, 12999 (2016).

[41] Y. X. Du, Z. Liang, Y. Li, X. Yue, Q. Lv, W. Huang, X. Chen, H. Yan, and S. Zhu, Nat. Commun. **7**, 12479 (2016).

[42] J. Zhang, J. H. Shim, I. Niemeyer, T. Taniguchi, T. Teraji, H. Abe, S. Onoda, T. Yamamoto, T. Ohshima, J. Isoya, and D. Suter, Phys. Rev. Lett. **110**, 240501 (2013).

[43] E. Torrontegui, S. Ibáñez, X. Chen, A. Ruschhaupt, D. Guéry-Odelin, and J. G. Muga, Phys. Rev. A **83**, 013415 (2011).

[44] J. G. Muga, X. Chen, S. Ibáñez, I. Lizuain, and A. Ruschhaupt, J. Phys. B **43**, 085509 (2010).

[45] E. Torrontegui, X. Chen, M. Modugno, A. Ruschhaupt, D. Guéry-Odelin, and J. G. Muga, Phys. Rev. A **85**, 033605 (2012).

[46] S. Masuda and K. Nakamura, Phys. Rev. A **84**, 043434 (2011).

[47] Y. H. Chen, Y. Xia, Q. Q. Chen, and J. Song, Phys. Rev. A **91**, 012325 (2015).

[48] X. Chen and J. G. Muga, Phys. Rev. A **82**, 053403 (2010).

[49] J. F. Schaff, P. Capuzzi, G. Labeyrie, and P. Vignolo, New J. Phys. **13**, 113017 (2011).

[50] X. Chen, E. Torrontegui, D. Stefanatos, J. S. Li, and J. G. Muga, Phys. Rev. A **84**, 043415 (2011).

[51] E. Torrontegui, X. Chen, M. Modugno, S. Schmidt, A. Ruschhaupt, and J. G. Muga, New J. Phys. **14**, 013031 (2012).

[52] A. del Campo, Eur. Phys. Lett. **96**, 60005 (2011).

[53] A. Ruschhaupt, X. Chen, D. Alonso, and J. G. Muga, New J. Phys. **14**, 093040 (2012).

[54] J. F. Schaff, X. L. Song, P. Vignolo, and G. Labeyrie, Phys. Rev. A **82**, 033430 (2010).

[55] J. F. Schaff, X. L. Song, P. Capuzzi, P. Vignolo, and G. Labeyrie, Eur. Phys. Lett. **93**, 23001 (2011).

[56] X. Chen and J. G. Muga, Phys. Rev. A **86**, 033405 (2012).

[57] M. Lu, Y. Xia, L. T. Shen, J. Song, and N. B. An, Phys. Rev. A **89**, 012326 (2014).

[58] Y. H. Chen, Y. Xia, Q. Q. Chen, and J. Song, Phys. Rev. A **89**, 033856 (2014).

[59] A. Baksic, H. Ribeiro, and A. A. Clerk, Phys. Rev. Lett. **116**, 230503 (2016).

[60] L. Giannelli and E. Arimondo, Phys. Rev. A **89**, 033419 (2014).

[61] S. Masuda and S. A. Rice, J. Phys. Chem. A **119**, 3479 (2015).

[62] M. G. Bason, M. Viteau, N. Malossi, P. Huillery, E. Arimondo, D. Ciampini, R. Fazio, V. Giovannetti, R. Mannella, and O. Morsch, Nat. Phys. **8**, 147 (2012).

[63] S. Martínez-Garaot, E. Torrontegui, X. Chen, and J. G. Muga, Phys. Rev. A **89**, 053408 (2014).

[64] T. Opatrný and K. Mømer, New J. Phys. **16**, 015025 (2014).

[65] H. Saberi, T. Opatrný, K. Mølmer, and A. del Campo, Phys. Rev. A **90**, 060301(R) (2014).

[66] E. Torrontegui, S. Martínez-Garaot, and J. G. Muga, Phys. Rev. A **89**, 043408 (2014).

[67] B. T. Torosov, G. Della Valle, and S. Longhi, Phys. Rev. A **87**, 052502 (2013).

[68] B. T. Torosov, G. Della Valle, and S. Longhi, Phys. Rev. A **89**, 063412 (2014).

[69] Y. H. Chen, Y. Xia, Q. C. Wu, B. H. Huang, and J. Song, Phys. Rev. A **93**, 052109 (2016).

[70] Y. H. Kang, Y. H. Chen, Q. C. Wu, B. H. Huang, Y. Xia, and J. Song, Sci. Rep. **6**, 30151 (2016).

[71] S. Ibáñez, X. Chen, E. Torrontegui, J. G. Muga, and A. Ruschhaupt, Phys. Rev. Lett. **109**, 100403 (2012).

[72] S. Ibáñez, X. Chen, and J. G. Muga, Phys. Rev. A **87**, 043402 (2013).

[73] X. K. Song, Q. Ai, J. Qiu, and F. G. Deng, Phys. Rev. A **93**, 052324 (2016).

[74] Y. Makhlin, G. Schön, and A. Shnirman, Rev. Mod. Phys. **73**, 357 (2001).

[75] C. P. Yang, Shih-I Chu, and S. Han, Phys. Rev. A **67**, 042311 (2003).

[76] C. P. Yang, Shih-I Chu, and S. Han, Phys. Rev. Lett. **92**, 117902 (2004).

[77] Y. Nakamura, Y. Pashkin, and J. S. Tsai, Nature (London) **398**, 786 (1999).

[78] A. Steinbach, P. Joyez, A. Cottet, D. Esteve, M. H. Devoret, M. E. Huber, and J. M. Martinis, Phys. Rev. Lett. **87**, 137003 (2001).

[79] J. M. Martinis and R. L. Kautz, Phys. Rev. Lett. **63**, 1507 (1989).

[80] R. Rouse, S. Han, and J. E. Lukens, Phys. Rev. Lett. **75**, 1614 (1995).

[81] C. H. van der Wal, A. C. J. ter Haar, F. K. Wilhelm, R. N. Schouten, C. J. P. M. Harmans, T. P. Orlando, S. Lloyd, and J. E. Mooij, Science **290**, 773 (2000).

[82] C. P. Yang and S. Han, Phys. Rev. A **74**, 044302 (2006).

[83] C. P. Yang, Q. P. Su, and S. Han, Phys. Rev. A **86**, 022329 (2012).

[84] C. P. Yang, Q. P. Su, S. B. Zheng, and S. Han, Phys. Rev. A **87**, 022320 (2013).

[85] Q.-P. Su, C.-P. Yang, and S.-B. Zheng, Sci. Rep. **4**, 3898 (2014).

[86] S. Han, R. Rouse, and J. E. Lukens, Phys. Rev. Lett. **76**, 3404 (1996).

[87] J. R. Friedman, V. Patel, W. Chen, S. K. Tolpygo, and J. E. Lukens, Nature (London) **406**, 43 (2000).

[88] D. Vion, A. Aassime, A. Cottet, P. Joyez, H. Pothier, C. Urbina, D. Esteve, and M. H. Devoret, Science **296**, 886 (2002).

[89] Y. Yu, S. Han, X. Chu, S. I. Chu, and Z. Wang, Science **296**, 889 (2002).

[90] I. Chiorescu, P. Bertet, K. Semba, Y. Nakamura, C. J. P. M. Harmans, and J. E. Mooij, Nature (London) **431**, 159 (2004).

[91] W. Dür, G. Vidal, and J. I. Cirac, Phys. Rev. A **62**, 062314 (2000).

[92] E. Jung, M. R. Hwang, Y. H. Ju, M. S. Kim, S. K. Yoo, H. Kim, D. K. Park, J. W. Son, S. Tamaryan, and S. K. Cha, Phys. Rev. A **78**, 012312 (2008).

[93] A. Karlsson and M. Bourennane, Phys. Rev. A **58**, 4394 (1998).

[94] Z. J. Deng, K. L. Gao, and M. Feng, Phys. Rev. A **74**, 064303 (2006).

[95] Z. L. Xiang, S. Ashhab, J. Q. You, and F. Nori, Rev. Mod. Phys. **85**, 623 (2013).